ELSEVIER

S0011-2275(96)00024-0

Cryogenics **36** (1996) 513–516

0011-2275/96/$15.00

A system dynamics model of split-type Stirling refrigerator

B.J. Huang, Y.P. Yang, F.M. Chen, S.B. Chien* and T.F. Shieh*

Department of Mechanical Engineering, National Taiwan University, Taipei 10764, Taiwan
*Chung-Shen Institute of Science and Technology, Lung-Tung, Taiwan

Received 3 October 1995; revised 8 January 1996

A non-contact and non-destructive technique was used to measure the displacer motion of a split-type Stirling refrigerator and the results were used to derive a system dynamics model. It is found that the split-type Stirling refrigerator is a third-order dynamic system with a zero. The parameters are shown to vary with the cold-end temperature. © 1996 Elsevier Science Limited ©1996 Elsevier Science Limited

Keywords: split-type Stirling refrigerator; dynamics model

Nomenclature

f	Frequency (Hz)
$G_{dp}(s)$	Transfer function
K	Steady-state gain
P_1	Pole
P_{ch}	Charge pressure (kg per cm^2 gauge, or MPa)
s	Laplace variable, complex
T_L	Cold-end temperature (K)
X_d	Displacer displacement (mm)
X_p	Piston displacement (mm)
Z_1	Zero

Greek letters

ξ	Damping ratio
ω	Angular frequency (rad s^{-1})
ω_n	Natural frequency (rad s^{-1})

The split-type Stirling refrigerator consists of a piston compressor and a cold finger that are connected by a connecting tube. The cold finger essentially includes a regenerator/displacer component, a gas spring and an expansion space (cold head) as shown in *Figure 1*. The displacer is driven by the pressure wave of helium gas resulting from the reciprocating motion of the piston. The cooling capacity depends on the amplitude variation and the phase shift of the pressure wave and the displacer displacement at the expansion space. The refrigeraor operates at a cyclically steady state due to the oscillating motions of the piston and the displacer that are very close to sinusoidal. The split-type Stirling refrigerator can thus be treated as a dynamic system with the piston displacement $X_p(t)$ as the system input and the displacer displacement $X_d(t)$ and the expansion space pressure $p_e(t)$ as the system outputs[1].

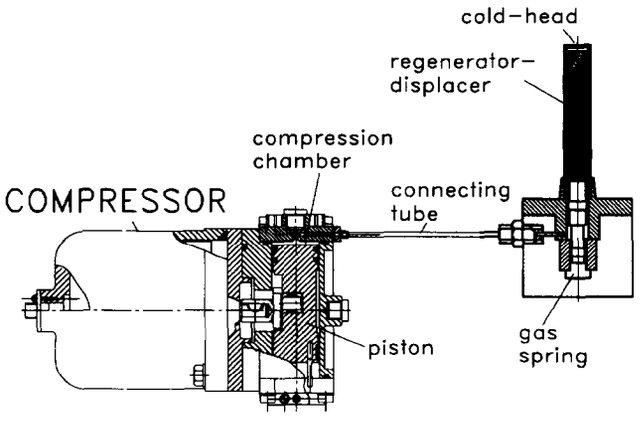

Figure 1 Schematic diagram of split-type Stirling refrigerator

Understanding the system dynamics model is very important in the control system design of Stirling refrigerators. Some researchers studied the control system design of a Stirling refrigerator experimentally by using a Hall-effect sensor[2,3] or an LVDT (linear variable-differential transformer) sensor[4,5] installed inside the refrigerator to detect the displacer motion for feedback control or dynamics modelling. A disturbance is thus introduced by the sensor attached to the displacer. The derived system dynamics model of the Stirling refrigerator is therefore inaccurate.

In the present study, we used a new non-contact and non-destructive measuring technique that utilizes an LVDT sensor mounted outside the cold finger to measure the displacer motion[6]. The results were used to derive a system dynamics model of the split-type Stirling refrigerator.

Table 1 Specifications of an experimental split-type Stirling refrigerator

1.	Piston stroke	12 mm	6.	Screen wire disks	700
2.	Piston diameter	26 mm	7.	Wire mesh	200 mesh
3.	Displacer diameter	12.7 mm	8.	Connecting tube diameter	1.3 mm
4.	Regenerator diameter	11 mm	9.	Connecting tube length	380 mm
5.	Regenerator length	60 mm	10.	Gas spring volume	1.0 cm^3

Experimental set-up

The LVDT non-contact displacer motion measurement system developed by Yang *et al.*[6] was used in the present experiment. A split-type Stirling refrigerator with crank-driven compressor was built for the experiment. The design specifications of the experimental Stirling refrigerator are listed in *Table 1*. The piston motion was measured by a Keyence LB70 laser measurement system. The laser beam was pointed directly at the bottom end of the piston through a transparent flange which was made of quartz. The displacement signals of the displacer and the piston were measured simultaneously by a Yokogawa YEW3655E multichannel high-speed recorder. A T-type thermocouple was used to measure the cold-end temperature and read by a YEW7563 recorder. All the signals were transmitted to a PC486 through an IEEE488 interface and the data were stored in disk for further analysis.

The 99.999% pure helium gas was charged to the refrigerator at 6 kg per cm^2 gauge (0.69 MPa) and the frequency was adjusted in the range 18–35 Hz. The cold finger was placed in a vacuum chamber which was evacuated to 10^{-5} torr by a diffusion pump so that the heat leak to the cold head is eliminated. The cooling capacity of the refrigerator was determined by measuring the DC current and the voltage across a heating resistance which was glued onto the cold-end surface. The testing conditions are listed in *Table 2*.

Derivation of system dynamics model

The system dynamics model of a split-type Stirling refrigerator can be represented by a transfer function which is the ratio of the displacer displacement to the piston displacement:

$$G_{dp}(s) = \frac{X_d(s)}{X_p(s)} \tag{1}$$

Since the motion of the displacer and the piston is approximately sinusoidal, the measured displacement signals $X_d(t)$, $X_p(t)$ can be used to directly compute the frequency response of the displacer-to-piston motion:

$$G_{dp}(j\omega) = \frac{X_d(j\omega)}{X_p(j\omega)} \tag{2}$$

The conversion of the transfer function in the s-plane $G_{dp}(s)$ from the frequency response function $G_{dp}(j\omega)$ can be achieved by simply replacing the angular frequency ω by s/j. This conversion is always assured by the linear system theory if the system is open-loop stable, which is the case for the split-type Stirling refrigerator.

A third-order model including a zero was proposed in the present study to correlate the experimental results:

$$G_{dp}(s) = \frac{K\left[\frac{s}{Z_1} - 1\right]}{\left(\frac{s}{P_1} - 1\right)\left[\frac{s^2}{\omega_n^2} + \frac{2\xi s}{\omega_n} + 1\right]} \tag{3}$$

where: K is the steady-state gain; Z_1 is the zero; P_1 is the pole; ω_n is the natural frequency of the displacer; and ξ is the damping ratio. The parameters were determined by fitting the frequency response data to Equation (3) by using a non-linear programming method[7]. It is shown from *Figures 2–7* that, the system identification is very good. The model parameters identified are listed in *Table 3*.

Discussion and conclusion

Figures 2 and *3* show the gain and phase at cold-end temperature 213 K. It is shown that the gain $|G_{dp}(j\omega)|$ has a peak value at 30 Hz with phase lag 90°. For a lower cold-end temperature at 193 K, the steady-state gain K increases

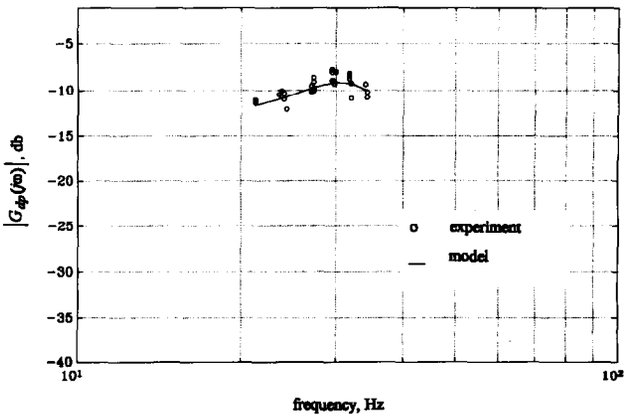

Figure 2 Gain of frequency response at cold-end temperature $T_L = 213$ K

Table 2 Testing conditions

Test No.	Cold-end temperature, T_L (K)	Charge pressure, P_{ch} (kg per cm^2 gauge)	Gas spring temperature (K)	Compression space temperature (K)	Frequency, f (Hz)
1	213	6	320	350	18.5–34.5
2	193	6	320	350	19–34.8
3	173	6	320	350	19–32.0

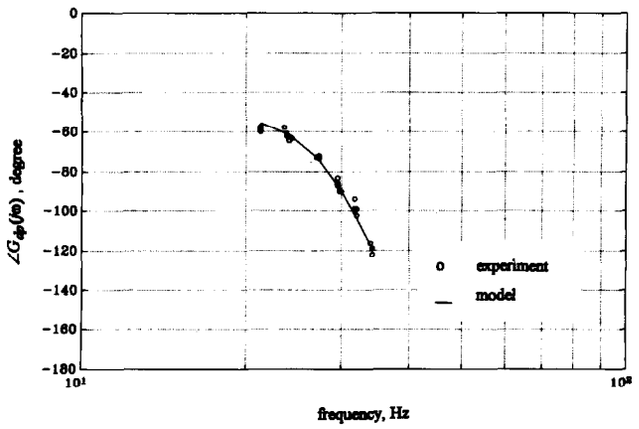

Figure 3 Phase of frequency response at cold-end temperature $T_L = 213$ K

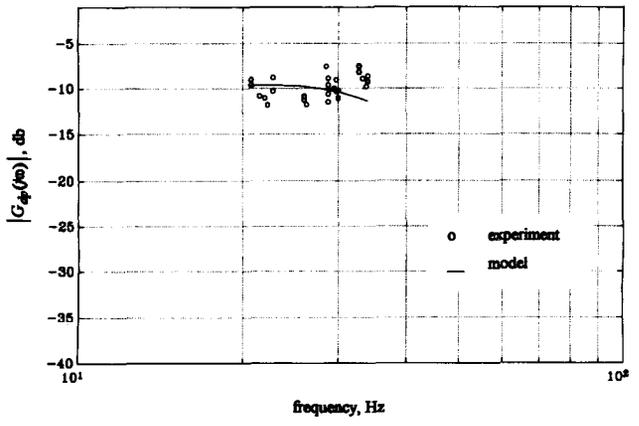

Figure 4 Gain of frequency response at cold-end temperature $T_L = 193$ K

but the peak value of the gain disappears as shown in *Figure 4*. The phase lag, however, decreases as shown in *Figure 5*. For the cold-end temperature at 173 K, both the steady-state gain K and the phase lag decrease, as shown in *Figures 6* and *7*.

The disappearance of the peak value in gain is probably caused by the variation of cylinder (cold-finger) diameter due to the cold-end temperature change. Since the displacer was made from fibre phenolic material and the cold finger from stainless steel 316L, different thermal shrinkage may occur as the temperature is lowered. A higher cold-end temperature thus results in a larger clearance between the displacer and cylinder wall and a small amount of friction. This can be verified by the identified parameters listed in *Table 3* in which the damping ratio ξ increases with decreasing cold-end temperature.

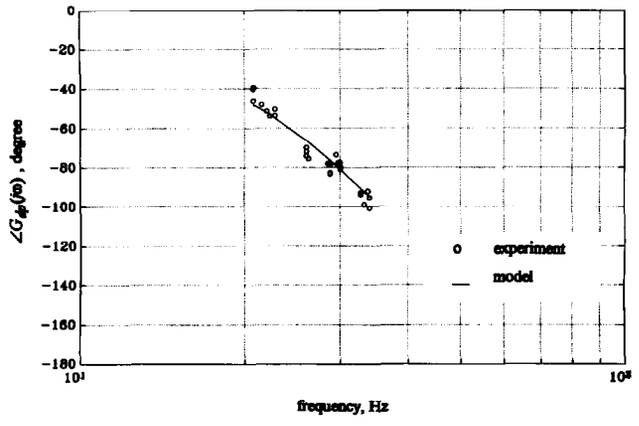

Figure 5 Phase of frequency response at cold-end temperature $T_L = 193$ K

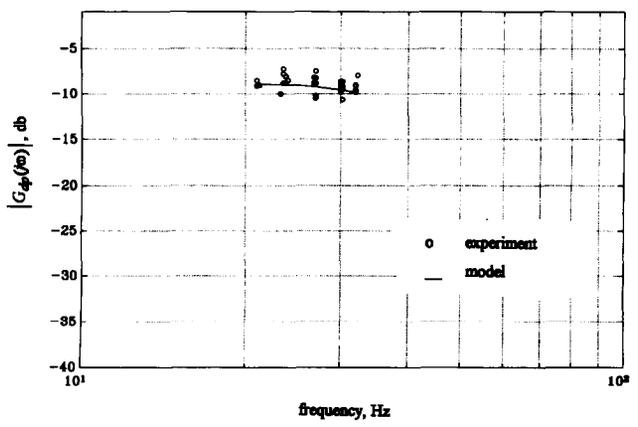

Figure 6 Gain of frequency response at cold-end temperature $T_L = 173$ K

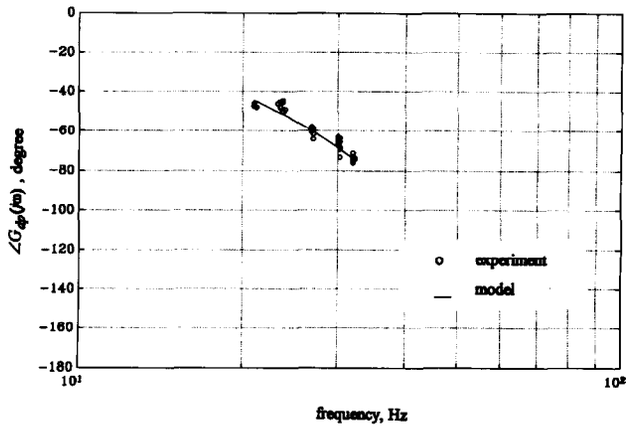

Figure 7 Phase of frequency response at cold-end temperature $T_L = 173$ K

The natural frequency ω_n, however, remains approximately constant for cold-end temperatures higher than 193 K, as shown in *Table 3*. The increase in ω_n at 173 K is probably due to variation in the gas spring constant caused by gas leakage through the seal.

The dynamics model derived in the present study has one pole and one zero in excess of the second-order model without zeros derived by some other researchers[2–5]. The additional zero Z_1 obtained in the present study is due to the dynamics behaviour of the regenerator in the process of energy storage/release. It usually has a fast response. The additional pole P_1 is due to the dynamics behaviour resulting from the fluid transport in the connecting tube. In deriving a dynamics model, former researchers[2–5] only considered the force balance of the displacer and com-

Table 3 System identification results

Cold-end temperature (K)	Gain K	Zero Z_1	Pole P_1	Damping ratio	Natural frequency
213	0.37	73.64	2.99	0.24	205.7
193	0.52	2.66	1.49	0.51	205.1
173	0.38	1.97	1.79	0.62	240.7

Table 4 Refrigerator performance at 213 K

Frequency (Hz)	19	21	23.8	27	29.5	31.9	34.2
Input power (W)	32.4	36.5	37.8	40	43	45	47.5
Cooling capacity (W)	0	0.47	0.67	1.38	1.95	2.41	1.76
Displacer stroke (mm)	2.96	3.33	3.49	4	4.52	4.27	3.95
Displacer phase lag (degrees)	53.9	58.3	62.1	72.8	87.6	98.9	119.1
COP	0	0.0129	0.0177	0.0345	0.0453	0.0536	0.0371

pletely ignored the effects of the regenerator and the connecting tube of the split-type Stirling refrigerator.

It is shown from *Table 3* that Z_1 decreases rapidly with decreasing cold-end temperature as the cold-end temperature starts to decrease from 213 K. For a cold-end temperature below 193 K, Z_1 decreases more slowly with cold-end temperature. From linear system theory, a system with a smaller zero will enhance the system response[8]. This indicates that the regenerator response is fast as the cold-end temperature decreases. This coincides with the experience that the regenerator should have a fast response in order to obtain a low cold-end temperature.

The pole P_1 is shown from *Table 3* first to decrease rapidly then increase slowly with cold-end temperature. This indicates that the fluid transport in the connecting tube is faster for lower cold-end temperatures. It was found from the present experiment that, at zero cooling load, the displacer stroke decreases as the cold-end temperature decreases, from 5.4 mm at 213 K to 3.2 mm at 173 K (both run at 33 Hz). The decrease in displacer stroke in turn reduces the gas mass flow rate through the regenerator as well as the connecting tube. The transport speed of gas through the connecting tube is thus reduced as the cold-end temperature decreases.

The refrigerator performances at a fixed cold-end temperature of 213 K were also measured and the results are presented in *Table 4*. The displacer stroke, cooling capacity and refrigerator COP (coefficient of performance) are all shown to increase with operating frequency, reach a maximum value at 31.9 Hz then decrease. The input power and the displacer phase lag increase monotonically with frequency. The optimum operating condition for the present refrigerator is at 31.9 Hz with cooling capacity 2.41 W and COP = 0.0536. This implies that the optimum performance of a split-type Stirling refrigerator depends on the operating conditions such as frequency and cold-end temperature, and the system design such as the regenerator, the displacer, the compressor, the connecting tube, etc. An optimum match should be obtained both in design and operating conditions in order to obtain a better performance.

Acknowledgement

The present study was supported by the National Science Council, R.O.C. through Grant No. CS84-0210-D-002-027.

References

1 **Huang, B.J. and Lu, C.W.** Linear network analysis of split-type Stirling refrigerator *Cryogenics* (1994) **34** (ICEC Suppl) 207–210
2 **Xiang Yu, Li Qing and Guo Fangzhong** Identification of the negative feedback relationship in split cycle free piston Stirling cryocooler system *Cryogenics* (1990) **30** (Sept Suppl) 216–220
3 **Li Qing, Xiao Jiahua, Guo Fangzhong and Wang Yuelan** Dynamic modeling of split cycle free piston Stirling cryocooler *Cryogenics* (1990) **30** (Sept Suppl) 211–215
4 **de Jonge, A.K.** A small free-piston Stirling refrigerator *14th IECEC* (1979) 1136–1141
5 **Stolfi, F. and de Jonge, A.K.** Stirling cryogenerators with linear drive *Phillips Tech Review* (1985) **42** 1–10
6 **Yang, Y.P., Chien, H.T. and Chen, J.M.** Non-contact measurement of displacer motion of a miniature split-Stirling cryocooler *Measurement* (1995) **14** 199–208
7 **Seidal, R.C.** Transfer-function-parameter estimation from frequency response data—a FORTRAN program, NASA Technical Memorandum NASA TM X-3286 (1975)
8 **Nagrath, I.J.and Gopal, M.** *Control Systems Engineering* Wiley Eastern Ltd, London (1985)